Automated Analysis of Ocean Surface Directional Wave Spectra

JEFFREY L. HANSON

The Johns Hopkins University Applied Physics Laboratory, Laurel, Maryland

OWEN M. PHILLIPS

The Johns Hopkins University, Baltimore, Maryland

(Manuscript received 21 September 1999, in final form 28 April 2000)

ABSTRACT

To facilitate investigations of surface wave processes in the open ocean, a wave spectral partitioning method with automated swell tracking and storm source identification capabilities has been developed. These tools collectively form the Wave Identification and Tracking System (WITS) and have been assembled entirely within the Matlab programming environment. A series of directional wave spectra, with supporting wind observations, is the only required input. Wave spectrum peaks representing specific wind sea and swell wave systems are extracted based on topographic minima, with wind sea peaks identified by wave age criteria. A swell tracking algorithm, combined with linear wave theory, provides a unique approach to storm source identification using the assimilated wave system statistics. The nature of the partitioned spectra allows the continuous, automated identification and tracking of multiple swell generation areas over space and time. Over a 6-day wave record in the Gulf of Alaska, 44 specific swell systems are identified, with up to three systems coexisting at any given time. The presence of atmospheric disturbances on surface weather charts validated the storm source predictions for more than 85% of these systems. The results are synthesized to depict the wave evolution history over the duration of the observations.

1. Introduction

Ocean surface waves generated by focused wind events have been observed to travel across ocean basins and even over 10 000 km from one ocean to another (Barber and Ursell 1948). Hence, the surface wave field at any point in a large ocean basin represents the sum of local wind sea and swell components propagating from distant storms. At particular times and locations, such as the winter storm period in the North Pacific Ocean, there are so many different wave systems propagating through any given region that the seas often appear totally confused.

Due to the complex nature of open-ocean surface wave conditions, extraction of meaningful information about specific wave systems and their storm sources from surface wave observations becomes a daunting task. Hence, directional wave spectra obtained from in situ and remote observations as well as from wave evolution models are often reduced to integrated statistical measures for wave field interpretations (IAHR Working Group on Wave Generation and Analysis 1989). These quantities, although useful for depicting trends in a particular series of observations, can greatly smear the essential attributes of a wave field when both wind sea and swell or multiple swell systems are present. Yet this information may significantly improve our ability to estimate air–sea exchanges and forecast surface wave conditions in shipping lanes and coastal areas.

In linear wave theory, wind episodes on the ocean surface produce a spectrum of waves that disperse according to the deep water dispersion relationship $f^2 = gk/(2\pi)^2$ between wave frequency (f), wavenumber (k), and acceleration of gravity (g). Wave energy travels at the group velocity $C_g = g/4\pi f$, which can be equated to the distance traveled divided by the travel time, $d/(t - t_0)$. For a wind event that was localized in time and space, the dominant wave frequency observed at some distant location linearly increases over time at a rate inversely proportional to the distance traveled:

$$\frac{df}{dt} = m_{ft} = \frac{g}{4\pi d}. \quad (1)$$

Remarkably, many wave events observed on the ocean behave in this fashion (Munk et al. 1963; Snodgrass et al. 1966). This dispersive nature allows one to extract information on the source of a particular wave system

Corresponding author address: Jeffrey L. Hanson, The Johns Hopkins University Applied Physics Laboratory, 11100 Johns Hopkins Road, Laurel, MD 20723-6099.
E-mail: jeffrey.hanson@jhuapl.edu

from measurements anywhere along their path of propagation, providing that the generation event is sufficiently localized in time and space. The distance to the wave source is simply

$$d = \frac{g}{4\pi m_{ft}}, \tag{2}$$

with the wave origination time calculated at $f = 0$ by

$$t_0 = -\frac{b}{m_{ft}}, \tag{3}$$

where b is the f intercept ($t = 0$) for the observed shift.

From swell frequency shifts observed at Cornwall, United Kingdom, Barber and Ursell (1948) verified that real waves in the deep ocean obey this dispersion law. Using bottom-mounted pressure gauge records, they identified storm sources at distances of 2200, 5100, and 11 100 km from their observation site. From similar observations off San Clemente Island, California, Munk et al. (1963) noted that individual swell systems form slanted ridges on frequency–time wave energy contour maps, with the time and great-circle distance to swell sources given by the slope and intercept of lines drawn along the ridges [Eqs. (2) and (3)]. Ridge-line plots from a series of 6 wave-observing stations along a great circle route between New Zealand and Alaska were used by Snodgrass et al. (1966) to resolve the source times and locations of 12 major swell events occurring over a period of 2½ months. Wave attenuation, determined using observations of the same event at the different stations, was negligible at frequencies below 0.07 Hz and 0.15 dB deg^{-1} at 0.08 Hz, where 1° = 60 nmi. They argue that swells are primarily attenuated by energy transfer through nonlinear interactions with other waves from the original storm. More recently, Mettlach et al. (1994) investigated swell propagation from Supertyphoon Flo in the North Pacific Ocean during September 1990. Using National Data Buoy Center (NDBC) buoy observations, they employed both the ridge-line technique and an approach of tracking spectral energy at two frequencies (Earle et al. 1984) to determine swell origin. They demonstrated that directional wave buoys could be used to provide the azimuth to the swell source, previously obtained only by triangulation from multiple observations. Most of these studies employed weather charts to determine if the predicted storm sources coincided with actual wind events on the ocean surface.

These studies clearly demonstrate that, in deep water, ocean swell propagates in general accordance with the deep-water simplifications to linear gravity wave theory. The effects of wave dissipation by breaking and molecular friction are minimal. Furthermore, distant storms can often be treated as point sources. The techniques are not without limitations, however. The storm source predictions are quite labor intensive; perhaps that is why none of these approaches has been successfully automated. The ridge-line method requires visual inspection of energy contour maps and hand-drawn lines. The two-frequency method is limited by the sample resolution; error is introduced if observations are not made at just the precise times, when the peak energy at each frequency passes the measurement site. In addition, there must be a frequency separation between individual swell events. This technique would not, for example, resolve the arrival of two swells at similar frequency from different directions. As a result, the previous studies have all focused on distinct swell events of relatively low frequency, primarily 0.08 Hz and below, and from extremely strong sources (e.g., Supertyphoon Flo).

Recently developed wave spectral partitioning approaches ought to facilitate a more convenient analysis of swell evolution and storm sources in the open ocean. Originally proposed by Gerling (1992), wave partitioning allows the identification and grouping of component wave systems from spatially and temporally distributed observations of directional wave spectra. A partitioning approach proposed by Hasselmann et al. (1994) has been implemented for comparison of *ERS-1* synthetic aperture radar image spectra with those obtained from WAM wave model predictions. They divide the spectra into subsets using an inverted catchment area approach. Wave height, frequency, and direction statistics, calculated for each subset, allow the evolution of multiple distinct wind sea and swell wave systems to be characterized across space and time with a greatly reduced set of spectral parameters. Recently, this technique has been extended by Voorrips et al. (1997) for the assimilation of wave observations into the WAM model.

Here, a wave spectral partitioning method, adapted from the approach of Hasselmann et al. (1994), is used to isolate distinct wind sea and swell wave statistics from directional wave spectra. These statistics are employed in a new, fully automated technique for analysis of wave climatology, including wave tracking and swell source predictions. Results from applying these techniques to data from a wave buoy in the North Pacific Ocean are presented.

2. Methodology

The isolation, tracking, and source identification of distinct wave systems is accomplished by the Wave Identification and Tracking System (WITS), a fully automated set of Matlab processing tools. This section summarizes the various methods employed. Additional details appear in Hanson (1996), with documentation of the data processing and graphic display capabilities appearing in Kline and Hanson (1995).

a. Spectral partitioning

Spectral partitioning facilitates the division of each directional wave energy spectrum $S(f, \theta)$ into distinct subsets that represent individual wind sea and swell wave systems. Each wave system is then conveniently

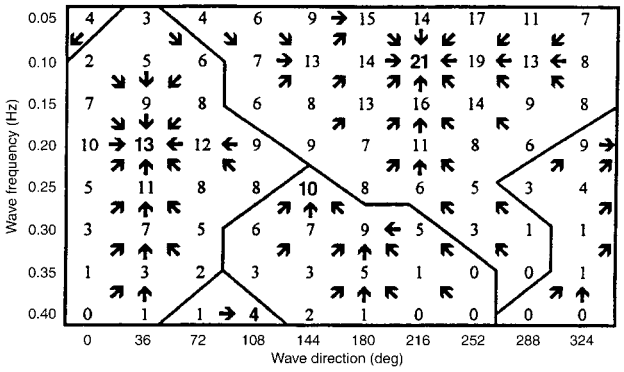

FIG. 1. Demonstration of spectral partitioning method. The paths of steepest ascent between each matrix value and the eight surrounding matrix neighbors are determined. The members that lie on the collection of paths that lead to the same local peak are then grouped to form a spectral partition.

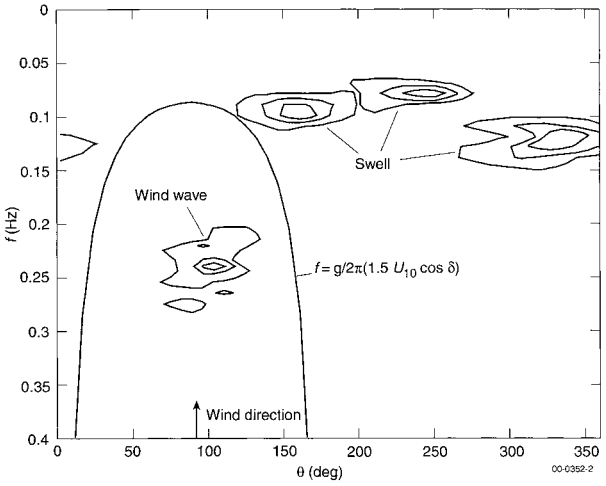

FIG. 2. Wind wave peaks are located within the parabolic region defined by the wave age criterion [Eq. (5)].

described by a reduced set of statistics. The concept was originally proposed by Gerling (1992); here the approach is based on the ideas of Hasselmann et al. (1994). The WITS partitioning of each input spectrum involves five steps, as outlined below.

STEP 1: PEAK ISOLATION

Search through the spectral matrix $S(f, \theta)$ and identify the paths of steepest ascent leading to each peak or local energy maximum. At each matrix value, check each of eight neighboring values (top, bottom, left, right, and diagonals) in this process. As depicted in the mock spectrum shown in Fig. 1, group all paths leading to the same peak as a distinct partition with a distinct partition number. A template matrix holds the partition number of every point in the spectrum and is saved as a separate file when all partitioning steps are complete. For each partition, determine the total energy e, the peak frequency f_p, the peak direction θ_p, and the peak energy $S(f_p, \theta_p)$. The peak frequency and direction are simply the coordinates of the peak in the energy spectrum.

STEP 2: IDENTIFY AND COMBINE WIND SEA PEAKS

Wind seas are identified using a wave age criterion such that wind sea peaks lie within the parabolic boundaries defined by

$$c_p \leq (1.5)U_{10} \cos\delta, \tag{4}$$

where c_p is the phase speed of the wind sea, U_{10} is the 10-m elevation wind speed, and δ is the angle between the wind and the wind sea. In terms of the peak frequency of the wind sea peak in deep water, (4) becomes

$$f_p \geq \frac{g}{2\pi}[1.5U_{10} \cos\delta]^{-1} \qquad 0 \leq \delta \leq \frac{\pi}{2}. \tag{5}$$

The generous factor of 1.5 ensures that all possible wind sea peaks are included. This relationship defines a parabolic region over the spectral matrix, as depicted in Fig. 2. Any partition whose peak falls within the region described by (5) is considered to be forced by the wind and initially defined as wind sea. All wind sea partitions from a given input spectrum are combined and assigned the partition number 0. All remaining partitions are considered swell.

STEP 3: COMBINE MUTUAL SWELL PEAKS

Adjacent swell peaks that belong to the same swell system are considered mutual and are combined. This is accomplished with user-supplied threshold factors and helps account for the noise inherent in discrete spectral estimates. To be considered mutual, two neighboring swell peaks must meet one of the following criteria.

Peak separation. Compare the distance between peaks

$$\Delta f^2 = (f_{px,1} - f_{px,2})^2 + (f_{py,1} - f_{py,2})^2,$$
$$f_{px} = f_p \cos\theta_p, \qquad f_{py} = f_p \sin\theta_p \tag{6}$$

with the spread of each individual peak

$$\overline{\delta f^2} = \overline{(f_x - \overline{f_x})^2} + \overline{(f_y - \overline{f_y})^2}$$
$$= \overline{f_x^2} - \overline{f_x}^2 + \overline{f_y^2} - \overline{f_y}^2, \tag{7}$$

where

$$\overline{f_x} = \overline{f \cos\theta} = \frac{1}{e}\int_f\int_\theta S(f, \theta) f \cos\theta \, \partial\theta \, \partial f,$$

$$\overline{f_y} = \overline{f \sin\theta} = \frac{1}{e}\int_f\int_\theta S(f, \theta) f \sin\theta \, \partial\theta \, \partial f,$$

$$\overline{f_x^2} = \overline{f^2 \cos^2\theta} = \frac{1}{e}\int_f\int_\theta S(f, \theta) f^2 \cos^2\theta \, \partial\theta \, \partial f,$$

$$\overline{f_y^2} = \overline{f^2 \sin^2\theta} = \frac{1}{e}\int_f\int_\theta S(f, \theta) f^2 \sin^2\theta \, \partial\theta \, \partial f,$$

with the integrations performed over the measurement domain and the total energy is given by

$$e = \iint S(f, \theta)\, d\theta\, df. \tag{8}$$

Combine the two peaks if the spread of either peak satisfies the peak separation criterion

$$\Delta f^2 \leq \kappa \overline{\delta f^2}, \tag{9}$$

where the spread factor κ is adjusted to optimize performance of the spectral partitioning. Optimization procedures are addressed in section 2d.

Minimum between peaks. Combine adjacent peaks if the lowest point between them is greater than the peak minimum factor ζ times the smaller of the two peaks. The peak minimum factor is also optimized for a particular observation set. Newly combined partitions are themselves eligible for further combinations, so all relevant partition statistics are updated whenever a combination is made.

STEP 4: ENERGY THRESHOLD CHECK

Remove any partitions whose total energy is below an energy threshold

$$e \leq \frac{A}{f_p^4 + B}, \tag{10}$$

where A and B are chosen to eliminate noise in low-energy regions of the spectrum (see section 2d). Note that this threshold includes the spectral fall-off proposed by Phillips (1985). Low-energy partitions are represented by negative ones in the template and are ignored for further processing. The remaining partitions are renumbered, and this information is saved to the partition template file. To conserve disk space, the partitioned spectra are not individually saved. The template files can be used at any time to extract spectral partitions from the original ''parent'' spectra.

STEP 5: CALCULATE PARTITION STATISTICS

For each of the final wind sea and swell partitions a variety of statistical information is calculated and saved to a partition statistics file. The contents of this file are described in the appendix.

b. Swell tracking

Swell tracking in WITS is a two-step process. First, preliminary groups of swell partitions likely to have been generated by the same source are formed. This is accomplished by grouping series of swell partitions with similar or slowly varying $\overline{f}$, $\overline{\theta}$, and a_{rms} characteristics. As swell arrives from a distant source, these attributes are expected to vary as a result of wave dispersion and storm source evolution. Preliminary wave tracking can be viewed as an initial sorting of swell partitions; groups are formed within which specific subsets, representing swells originating from distinct localized weather events, can be sought.

To determine if a new swell partition belongs with a previously identified preliminary group, the location of the new partition in a weighted frequency–direction–height space is compared to a predicted group location computed from the average properties of the previous five partitions in each existing group. If the group contains fewer than five partitions, then all of the partitions are used in determining the group location. The weighted distance between a new observation and the predicted group value is given by

$$d = \sqrt{\left(\frac{a_{\text{rms,peak}} - a_{\text{rms,group}}}{3a_{\text{rms,group}}}\right)^2 + \left(\frac{\theta_m - \theta_{\text{group}}}{\pi}\right)^2 + \left(\frac{\log f_m - \log f_{\text{group}}}{\frac{1}{3}}\right)^2}, \tag{11}$$

where θ is in radians and the coefficients have been introduced to emphasize the relative importance of each term. The new observation is assigned to the group with which it shares the smallest value of d. Values of d greater than an assigned threshold are considered too high for a valid match. When a partition cannot be assigned to an existing group, a new group is created for it. The weighting factors in (11) have been selected through an iterative trial and error process. Although they work well, we anticipate employing more efficient clustering techniques in future upgrades of WITS.

The second step locates specific swell events within preliminary groups. A specific event is an evolving set of swells that were formed at the same time and location. The events are located by searching through the preliminary wave groups for series that obey deep-water wave dispersion characteristics. Each preliminary group is searched as a whole to find embedded specific groups. The slope and variance about the best-fit line through all possible sequences of three or more observations is determined. Both slope and variance thresholds are employed to discriminate against swells that do not exhibit

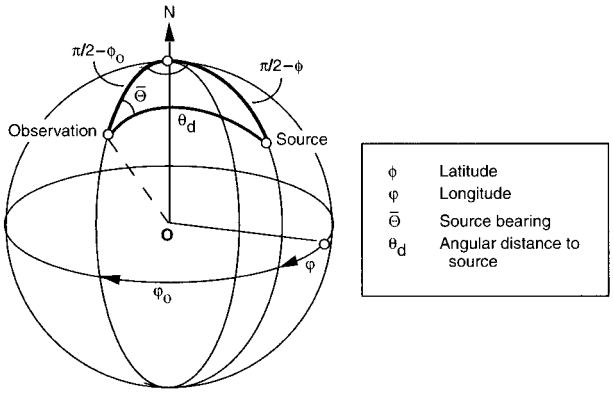

FIG. 3. Great circle geometry for calculation of swell locations.

the required dispersion characteristics. The longest possible sequences whose slopes and variance fall within the threshold limits are considered specific swell systems (Kline and Hanson 1995).

c. Swell source identification

The resulting wave partitions allow automated identification and tracking of multiple storm systems. A distinct swell source time and location is calculated from each specific group of swell partitions. The slope and intercept of the best-fit line through the mean frequency and time data pairs $(\overline{f}, t)$ are used in the linear gravity wave theory simplifications of Eqs. (2) and (3) to determine the distance to the swell source and the swell origination time, respectively. A specific group mean wave direction $\overline{\Theta}$, obtained by averaging the $\overline{\theta}_s$ values from all group members, is used to indicate the great-circle route over which the waves have traveled. The source location is then obtained by spherical geometry. As depicted in Fig. 3, the wave observation site, the North Pole, and the swell source location all form a spherical triangle on the surface of the earth. The source latitude (ϕ) and longitude (φ) are then given by (Bartsch 1974):

$$\phi = \sin^{-1}(\sin\phi_o \cos\theta_d + \cos\phi_o \sin\theta_d \cos\overline{\Theta}),$$

$$\varphi = \varphi_o - \sin^{-1}\left(\frac{\sin\theta_d \sin\overline{\Theta}}{\cos\phi}\right), \quad (12)$$

where ϕ_0 = observation latitude, φ_0 = observation longitude, $\theta_d = (d/R_E)$ = angular distance to source, and R_E = radius of the earth. Once the swell generation times and locations are determined, they are located on regional weather maps to determine the credibility of each prediction.

d. Parameter selection

The success of the WITS partitioning process is dependent upon proper selection of the various adjustable parameters. These parameters are chosen to optimize the performance of the partitioning, tracking, and storm source identification algorithms on a given observation set. The need for adjustable parameters arises primarily from variations in regional wave climatology, although differing frequency and direction resolutions and instrument noise levels can contribute. The described methods have been applied to the datasets listed in Table 1. Included are data from several different instruments as well as a wave model; these observations and predictions cover a wide variety of climatic environments. The parameters listed in Table 1 were chosen through iteration to optimize the wave system identifications and storm source predictions of each set.

The minimum energy threshold parameters A and B from Eq. (10) are the most crucial, as the spectral noise floor is a function of the wave climate at a given site. This is demonstrated by the computed threshold levels from the Datawell WAVEC buoy observations in the North Pacific Ocean and the Gulf of Mexico. The smaller values from the Gulf of Mexico are a result of a much calmer wave environment, which effectively lowered the instrument noise floor. The WITS toolkit includes a utility for optimizing the selection of A and B. As demonstrated in Fig. 4, the utility places the energy threshold curve (10) over a plot of the total energy of each isolated partition as a function of peak frequency. The values of A and B are then easily adjusted based on output sensitivity requirements and the noise floor of the dataset.

The peak combination parameters κ and ζ are selected through iteration to optimize both the selection of distinct wave systems and the prediction of storm source locations. One measure of performance is the mean regression coefficient from the specific swell group linear correlations of mean frequency versus time (see section 2c). Another is the percentage of storm source predictions that can be verified on surface weather charts. Note

TABLE 1. Observation sets that have been analyzed using the spectral partitioning method.

Observations			Selected parameters			
Location	Date	Source	A	B	κ	ς
North Pacific	Feb 1992	Datawell WAVEC buoy	6×10^{-5}	2×10^{-3}	0.4	0.65
Gulf of Mexico	Nov 1995	Datawell WAVEC buoy	2×10^{-6}	3×10^{-2}	0.4	0.65
Gulf of Mexico	Nov 1995	NDBC Buoy #42036	2×10^{-6}	3×10^{-2}	0.4	0.65
Mid-Pacific (HI)	Feb 1997	Datawell Waverider buoy	6×10^{-6}	3×10^{-3}	0.4	0.65
North Pacific	Aug 1998	Wave Model WAM	4×10^{-5}	2×10^{-3}	0.5	0.75

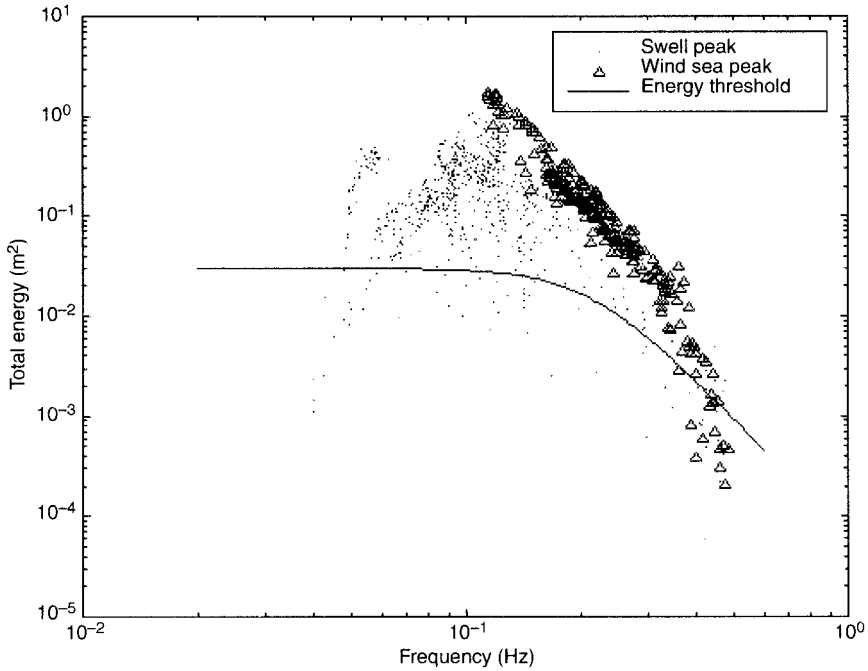

FIG. 4. Minimum energy threshold applied to Feb 1992 observations in the North Pacific Ocean. Swell partitions whose total energy falls below the energy threshold $A/(f_p^4 + B)$ are discarded.

that the same values of κ and ζ were selected in all of the field datasets in Table 1; only the WAM model predictions required slightly adjusted parameters to optimize peak combinations.

In combining swells with preliminary groups, the weighted distance, d in amplitude–direction–frequency space is determined by (11). A threshold for d allows for discrimination between different swell sources. For the observations reported here, a value of $d = 0.6$ provided the best performance in forming preliminary groups. The performance of this threshold is evaluated by plotting the evolution of wave vectors or wave vector history. An example is provided in section 4. Discontinuities in evolving swell systems would indicate that d needs to be increased; the inclusion of disparate wave systems in the same group would indicate the opposite.

3. Gulf of Alaska observations

To demonstrate the performance of the spectral partitioning, swell tracking, and storm source identification methods, results from the North Pacific observation set in Table 1 will be discussed. These data were collected during the Gulf of Alaska Surface Scatter and Air–Sea Interaction Experiment (Hanson and Erskine 1992), which was the seventh cruise within a series of Critical Sea Test Experiments conducted for the U.S. Navy (Tyler 1992). The observations included wind and wave measurements obtained from 24 February through 1 March 1992 in the central Gulf of Alaska at approximately 48°45′N, 150°00′W.

a. Measurements

Atmospheric and sea surface measurements were obtained by a MINIMET meteorological buoy (Coastal Climate Company) deployed from R/V *John P. Tully*. The instrument was outfitted with a drogue at a depth of 165 m to minimize advection by near-surface currents and was allowed to drift within the test site. Observations obtained at 1-Hz resolution included wind speed and direction at 3-m height, air temperature, sea surface temperature, and barometric pressure. MINIMET data were processed using a marine atmospheric boundary layer model (Smith 1988) to generate surface layer profiles, adjust meteorological measurements to common reference elevations, and compute atmospheric stability parameters and wind stress (Hanson and White 1991). Output quantities were averaged to form 30-min values that coincide with the surface wave observations. Vector-averaged wind speed estimates at 10-m height (U_{10}) are used for the results reported here. These observations compared well with those obtained by a nearby shipboard meteorological station (Hanson et al. 1993).

Continuous measurements of wave height and direction over the experimental period were taken by a Datawell WAVEC heave, pitch, and roll buoy deployed from the *John P. Tully* (Farmer 1992). The instrument was drogued at a 100-m depth and allowed to drift with the surface currents. Although not required for this analysis, this deployment approach reduced wave Doppler contamination by surface currents and also stabilized the buoy against capsizing. Surface displacement and

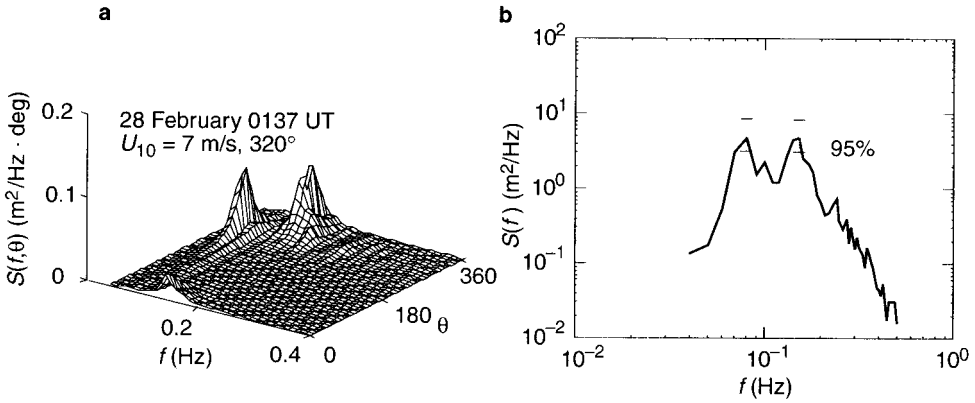

FIG. 5. Example Gulf of Alaska wave spectrum from 0137 UTC 28 Feb 1992. (a) Full-directional (2D) wave spectrum, and (b) one-dimensional (1D) wave spectrum with 95% confidence intervals.

vector slope were sampled at 1.28 Hz and transmitted to a receiver aboard the *John P. Tully*. A few record gaps, of several hours duration, occurred when the buoy drifted out of telemetry range from the ship.

Wave statistics and a total of 236 half-hourly directional spectra were computed by Juszko et al. (1995) using a data-adaptive eigenvector (EV) technique (Marsden and Juszko 1987). Spectra containing 36 degrees of freedom were computed over the frequency band $0.05 \leq f \leq 0.5$ Hz to obtain estimates over the range that the wave buoy is considered most accurate. A particularly attractive aspect of the EV method for this investigation is an exceptional resolution of individual peaks within multimodal spectra such as those obtained from the Gulf of Alaska.

Typical directional (2D) and one-dimensional (1D) wave spectra from a single 30-min wave record from this study appear in Figs. 5a and 5b, respectively. The directions reported are the directions from which the waves are propagating. The directional spectrum has two large peaks, indicating a wind sea from the northwest coexisting with a lower-frequency swell from the west. These two events also appear as isolated peaks on the 1D spectrum, calculated using

$$S(f) = \int_0^{2\pi} S(f, \theta)\, d\theta. \tag{13}$$

The 95% confidence intervals in Fig. 5b indicate that the wind sea and swell wave peaks are distinct wave events (Shumway 1988).

b. Experimental conditions

The winter weather we experienced was influenced by four separate atmospheric low pressure systems moving through the North Pacific region. Selected meteorological and sea surface records from the experiment appear in Fig. 6. The first two lows, occurring on 24 and 26 February, passed almost directly over the test site and had the most significant impact on meteorological conditions. Note in particular the rapid air temperature changes due to the atmospheric fronts associated with these two lows. A notable amount of local variability in wind speed and direction existed (Fig. 6), with high-wind events associated with each passing storm. The most significant of these were the two approximately 12-h wind episodes associated with the 25–26 February winter storm. The structure of this storm as it passed northward over the test site at a speed of approximately 12 m s^{-1} is depicted by the National Oceanic and Atmospheric Administration (NOAA) surface pressure map series of Fig. 7. This single low pressure cell dominated the weather in nearly the entire gulf for a period of approximately 36 h.

Of particular importance for this study was the effect these meteorological events had on the wave field. The significant wave height record of Fig. 6 indicates that surface waves peaked at 5.3 m as a result of the 25–26 February storm. Wave heights did not develop as dramatically during the other high-wind events because the winds were either too low, too unsteady, or too variable in direction. However, even during times of low winds, significant wave heights were at least 2 m because of ocean swells propagating through the gulf. In fact, the continual arrival of long-period swell from remote weather events, often at considerable angles to the wind waves, led to a ''confused sea'' visual appearance during much of the test.

4. Results: Swell evolution in the Gulf of Alaska

The automated partitioning and tracking of wave systems from the 236 directional wave spectra resulted in the identification of numerous distinct wind sea and swell events that passed through the Gulf of Alaska test site. These events were found to be a consequence of the atmospheric low pressure cyclones that rapidly evolve across the North Pacific Ocean during winter. We concentrate here on the swells of nonlocal origin, which are generally superposed upon

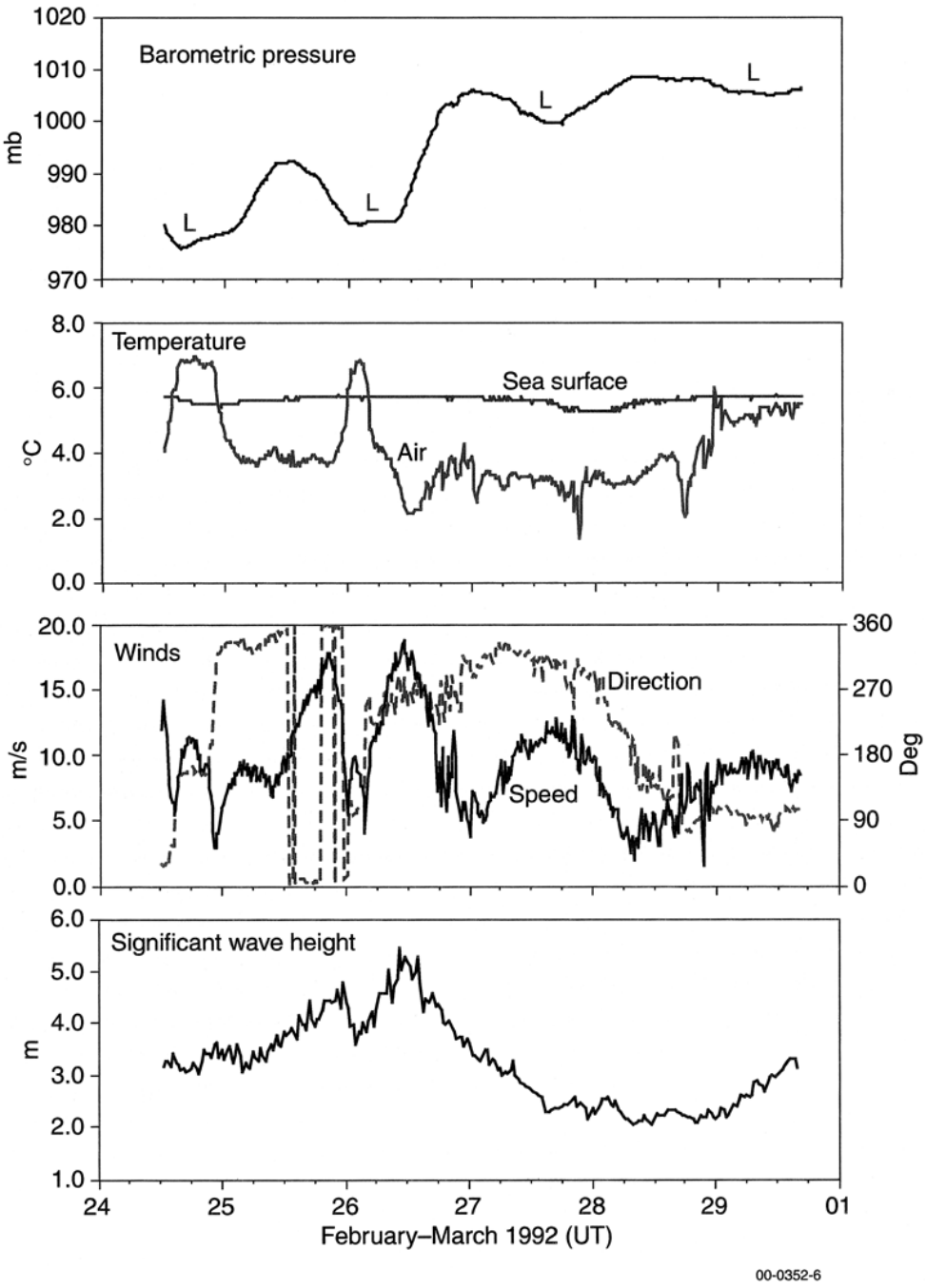

FIG. 6. Selected meteorological and sea surface records from Gulf of Alaska experiment.

and may be obscured in visual observation by the local wind seas.

a. Swell systems

The results of the Gulf of Alaska preliminary wave tracking appear in the wave vector history plot of Fig. 8. Swell mean frequency $\overline{f}$, rms height, and propagation direction are given by vector origin, length, and azimuth, respectively. Preliminary groups are color coded and numbered. Note that wind seas, isolated using the wave age criterion [Eq. (5)], do not appear on these figures; they are discussed briefly at the end of this section.

The swell events depicted in Fig. 8 are essentially tracers of local and distant storms traveling through the North Pacific. Perhaps the most striking feature is that at any given time, there were at least two, and often

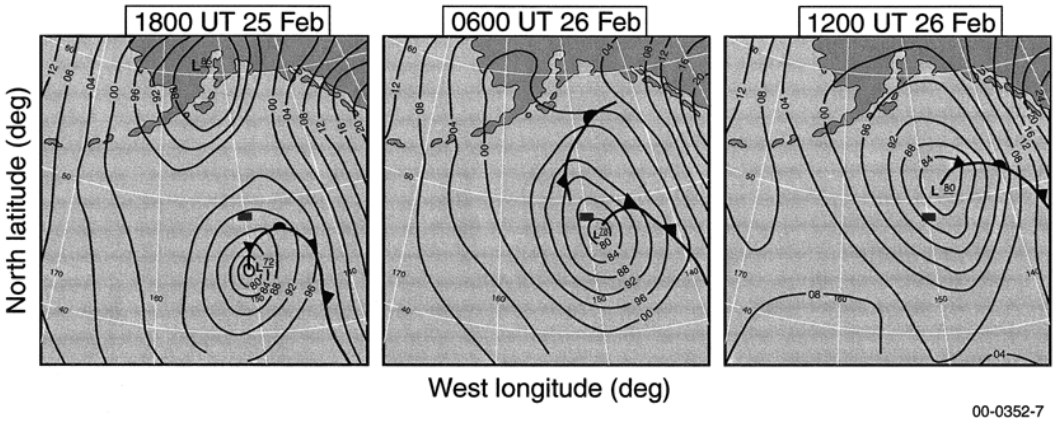

FIG. 7. NOAA surface pressure maps showing a large North Pacific low pressure storm passing directly over the test site on 25–26 Feb 1992 (UTC). Peak winds of 18 m s^{-1} and significant wave heights of 5.3 m resulted from this event.

three, simultaneous swell systems evolving through the Gulf of Alaska. Swells within the lower-frequency groups (shown in red) had presumably traveled the farthest distance; their directions suggest they propagated into the Gulf of Alaska from the wide-open Pacific basin. These groups exhibit a linear frequency increase with time, as predicted by the wave–dispersion relationship [Eq. (1)]. It is shown later that the higher-frequency groups contain subsets that exhibit this same behavior. Two midfrequency groups (shown in magenta and cyan) persisted for nearly 3.5 days from the start of observations on 24 February until a record gap just before 1200 UTC on 27 February. The swell events in these groups nearly always opposed each other in direction and shifted forward and back within a narrow frequency range of approximately 0.09–0.13 Hz. The green groups have some members at fairly high frequency for swell. These events are correlated with abrupt changes in the wind forcing; very young, local swells persist for a short time after the wind shifts.

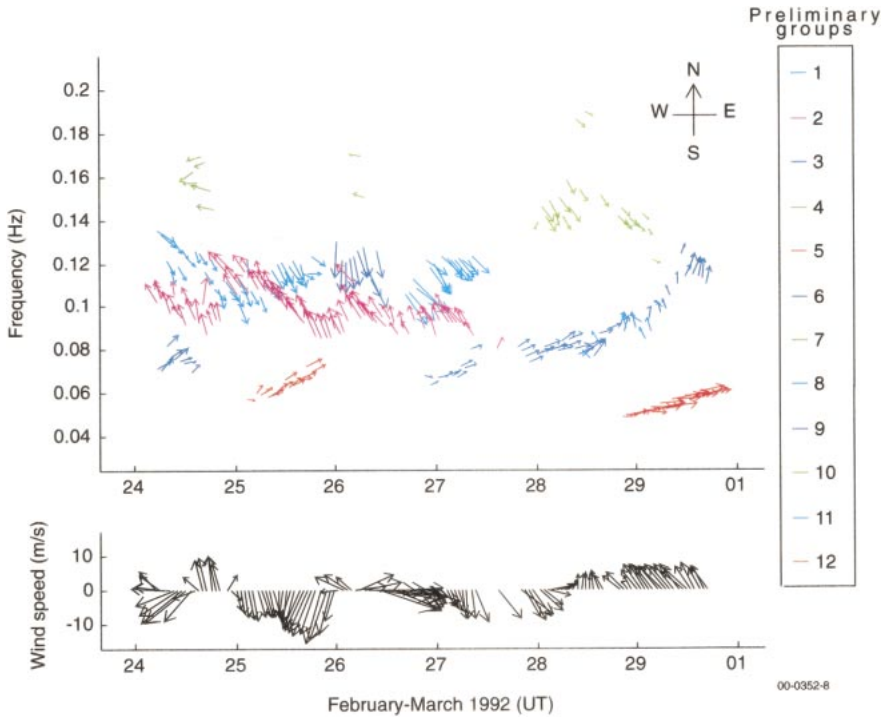

FIG. 8. Wave vector plot of preliminary swell groups. Vector origin, length, and azimuth represent swell frequency, rms wave height, and swell propagation direction, respectively. Sequential color coding is from high frequency to low frequency and from left to right.

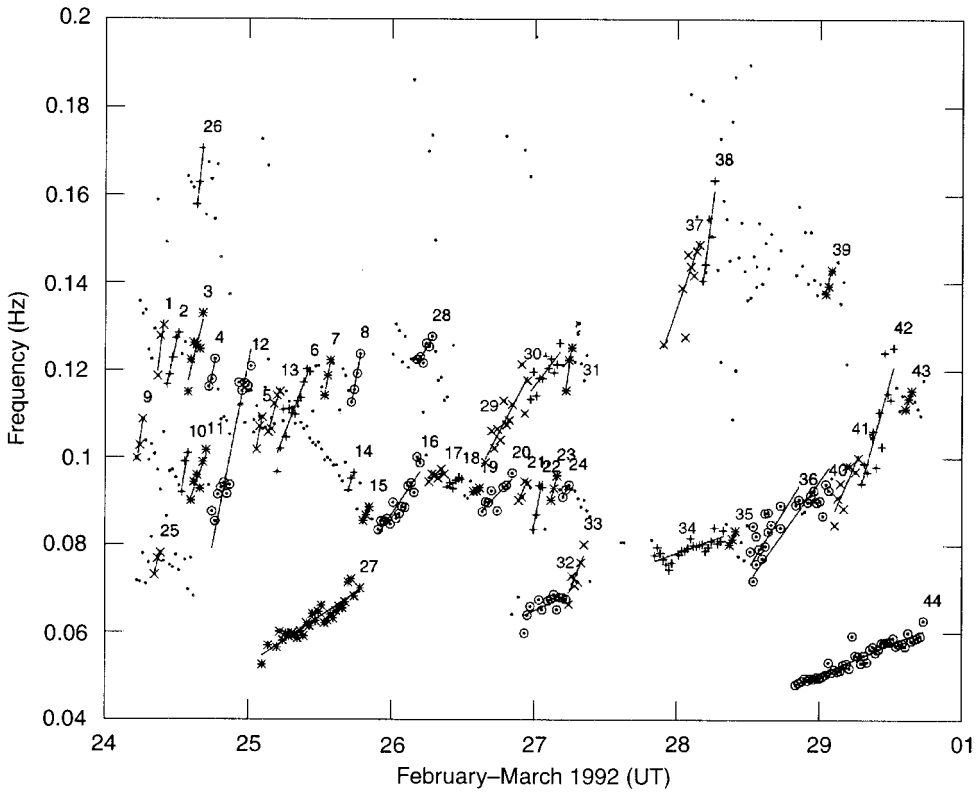

FIG. 9. Swell partition mean frequency vs time with specific swell groups numbered and identified with enlarged symbols and linear regressions. As dictated by wave dispersion, all specific wave groups shift upward in frequency over time.

The swell tracking algorithm identified 19 original preliminary groups. The seven groups that do not appear in Fig. 8 were eliminated because they contained only three partitions, each with extremely low energy levels. It could not be determined if these observations were poorly resolved swell events or just sampling noise. These discarded partitions represent less than 1% of the total amount of partitioned swell energy.

b. Storm source predictions

Specific wave tracking was performed on each preliminary group from the Gulf of Alaska observations. A total of 44 specific swell events were identified in the 6-day wave record. These events are shown on the frequency evolution plot in Fig. 9. Here, the mean frequency of each swell partition is plotted as a function of observation time. Specific swell groups are numbered and depicted with enlarged symbols. A least squares regression line is drawn through each specific group. A very good correlation exists for each group, with $r = 0.9$ being the average correlation coefficient for the entire set.

Note that in Fig. 9, not all members of each preliminary group fall into a specific swell group. The unselected partitions (identified by small dots) contain about 35% of the total swell energy that passed by the observation site during the 6-day measurement period. These are valid swell events that do not exhibit the dispersive characteristics predicted by linear wave theory. They may have originated with events that are not well represented as point sources, such as fast-moving storms or steady, continuous wind. These events will result in a less focused dispersive signal at a distant observation point. Furthermore, interactions between frequency components from the same storm, interactions with wind and sea from other meteorological events along the route, and refraction by major ocean currents may all contribute to the attenuation and scattering of the original swell. Thus across ocean basins only selected windows of opportunity may allow swell systems to pass unaltered; these are represented by the specific groups in Fig. 9.

As wave dispersion dictates, the specific groups in Fig. 9 all display a steady increase of wave frequency with time. Only the slope and intercept of each regression line and the mean direction of each series are required to predict the swell generation times and locations using Eqs. (2), (3), and (12). The storm parameters of all 44 specific swell events are listed in Table 2. This information was directly obtained from the automated processing of the directional wave spectra. The $(\overline{f}, t)$

TABLE 2. Specific swell system storm source parameters.

Specific group	m_{ft}	b	$\overline{\Theta}$	t_0	d (km)	ϕ (+N/−S)	φ (+W/−E)	Weather map detection	Swell source
1	0.278	−6.648	−29	23.9	243	50.647	151.671	Direct	Local storm
2	0.153	−3.617	−22	23.7	441	52.405	152.433	Direct	Local storm
3	0.132	−3.136	−34	23.7	509	52.453	154.254	Direct	Local storm
4	0.152	−3.634	−34	23.9	444	52.009	153.635	Direct	Local storm
5	0.177	−4.322	−24	24.5	382	51.877	152.223	Inferred	Local storm
6	0.086	−2.056	−29	24.0	788	54.783	156.021	Direct	Local storm
7	0.193	−4.822	−26	24.9	349	51.537	152.246	Direct	Local storm
8	0.177	−4.447	−59	25.1	380	50.43	154.599	Direct	Local storm
9	0.214	−5.071	155	23.7	316	46.172	148.235	Direct	Stationary blocking high
10	0.214	−5.146	155	24.1	316	46.163	148.267	Direct	Approaching storm
11	0.093	−2.2	165	23.6	724	42.446	147.661	Direct	Stationary blocking high
12	0.168	−4.082	155	24.3	401	45.46	147.833	Direct	Approaching storm
13	0.125	−3.024	146	24.3	542	44.635	146.196	Direct	Approaching storm
14	0.098	−2.425	149	24.7	688	43.36	145.604	Inferred	Stationary blocking high
15	0.074	−1.821	154	24.6	913	41.268	145.207	Direct	Stationary blocking high
16	0.049	−1.191	160	24.2	1372	37.045	144.62	Direct	Stationary blocking high
17	0.016	−0.316	146	20.2	4308	14.061	129.038	Inferred	Stationary blocking high
18	0.019	−0.416	150	21.6	3498	20.045	133.941	Inferred	Stationary blocking high
19	0.020	−0.445	165	22.0	3338	19.376	142.308	Inferred	Stationary blocking high
20	0.035	−0.833	158	24.1	1950	32.144	142.483	Inferred	Stationary blocking high
21	0.073	−1.884	160	25.7	918	40.938	146.199	Direct	Approaching storm
22	0.172	−4.554	163	26.5	392	45.369	148.513	Inferred	Stationary block high
23	0.135	−3.581	145	26.4	498	45.022	146.362	Inferred	Stationary blocking high
24	0.066	−1.699	146	25.8	1025	40.857	143.265	Direct	Stationary blocking high
25	0.122	−2.886	−122	23.7	555	45.908	156.052	None	Unknown
26	0.302	−7.274	77	24.1	224	49.169	147.005	Direct	Approaching storm
27	0.022	−0.491	−122	22.6	3102	30.201	177.487	Direct	Mid-Pacific storm
28	0.052	−1.246	−14	23.8	1291	59.893	155.649	None	Unknown
29	0.064	−1.604	−42	25.1	1055	55.297	161.212	Direct	Local storm
30	0.043	−1.038	−33	24.3	1577	59.733	165.551	None	Unknown
31	0.236	−6.294	−40	26.7	286	50.7	152.604	Direct	Local storm
32	0.015	−0.349	−113	22.8	4405	24.438	−169.908	Inferred	Fast-moving mid-Pacific storm
33	0.082	−2.169	−102	26.4	821	46.679	160.543	Inferred	Stationary mid-Pacific storm
34	0.012	−0.26	−111	21.5	5593	17.355	−161.181	None	Unknown
35	0.075	−2.048	−117	27.3	899	44.627	160.157	Inferred	Stationary mid-Pacific storm
36	0.053	−1.438	−132	27.1	1270	40.571	161.263	Direct	Mid-Pacific storm
37	0.094	−2.5	−18	26.6	717	54.82	153.522	Direct	Local storm
38	0.248	−6.851	−29	27.6	272	50.882	151.855	Direct	Local storm
39	0.108	−3.004	−51	27.8	623	52.08	157.082	Direct	Local storm
40	0.047	−1.256	140	27.0	1448	38.243	139.333	Direct	Approaching storm
41	0.076	−2.137	151	27.9	882	41.675	144.891	Inferred	Approaching storm
42	0.117	−3.329	178	28.5	577	43.564	149.73	Direct	Approaching storm
43	0.1	−2.856	−164	28.5	673	42.907	152.258	Direct	Approaching storm
44	0.014	−0.341	−99	25.3	4995	27.387	−158.214	Direct	Western Pacific storm

regression slope m_{ft} and intercept b are listed along with the mean wave propagation direction $\overline{\Theta}$ for each specific group. The calculated swell origination time t_0, distance traveled d, and source geographic coordinates (ϕ, φ) are also provided in Table 2.

The last two columns of Table 2 provide comments pertaining to the identification of the predicted source storms on National Weather Service (NWS) regional surface pressure charts. A direct detection indicates that a storm was found at the predicted time and location with winds oriented toward the observation site. Wind orientations are assumed to be parallel to the isobars, with cyclonic rotation about low pressure centers in the Northern Hemisphere. Inferred detections suggest that a storm occurred in the general region of the predicted site within ±12 h of the predicted observation time. This makes allowances for 1) slight modifications to the propagating swell by the processes discussed above; 2) inaccuracies in the weather charts, which are based on sparsely distributed observations; and 3) noise inherent in the collection and processing of the wave data. As Table 2 indicates, most of the inferred sources were either stationary features or quickly moving storms. In a few instances, no detections were made, suggesting that either an erroneous specific group was selected or the storm was missed on the NWS chart. Of the total swell energy in the 44 specific groups, 70% arrived from directly detected sources, 16% was from inferred sources, and 14% was of unidentifiable origin. The process of identifying swell sources using predicted parameters and NWS charts is illustrated below, with a few examples from Table 2.

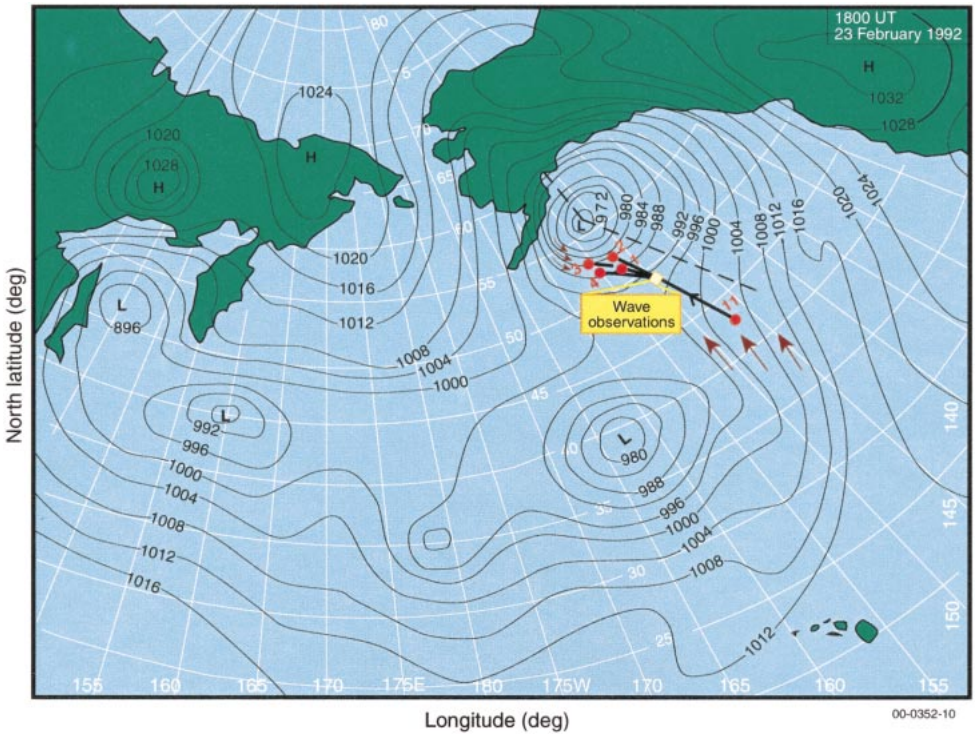

FIG. 10. National Weather Service surface pressure chart for 1800 UTC 23 Feb 1992. Predicted source locations and great circle propagation routes are displayed for specific groups 1, 2, 3, 4, and 11.

Specific groups 1, 2, 3, 4, and 11 have t_0 that fall in the latter part of 23 February 1992. The corresponding source locations (ϕ, φ) are plotted on the North Pacific surface pressure chart for 1800 UTC 23 February 1992 in Fig. 10. The great circle paths that connect the source locations with the wave observation site are also shown on the chart. Note that a single low pressure storm centered directly in the Gulf of Alaska is responsible for swell groups 1–4. The predicted source positions are located precisely where the cyclonically rotating winds would be expected to generate waves directed toward the wave observation site. These are essentially young swell events that have traveled distances of 243–509 km (Table 2).

The predicted source for swell group 11 is 724 km south of the observation area in a wide swath of increasing pressure to the east (Fig. 10). As with the previous groups, the source is located precisely in a region where wave generation would be directed toward the observation site. As this pressure ''wall'' was a semistationary feature on the weather charts from 22 February 1992 to 26 February 1992, many of the specific groups evolving from this direction did not exhibit a clear dispersive trend.

In contrast to the swell from meteorological events in the general region of the Gulf of Alaska, wave groups 27 and 32–36 all appear to be a result of distant storms moving across the Pacific basin (Table 2). The swell from these events have predicted travel distances of 1000–5000 km or more. Specific group 27 is a particularly clear example of these waves. The predicted source location for specific group 27 appears on the 22 February 1992 (1200 UTC) weather chart reconstruction of Fig. 11. The source is located to the southeast of a large low-pressure system in a region of significant wind fetch well away from the storm center.

Specific swell groups 8, 21, and 44 are all predicted to have been generated on 25 February 1992, but at widely separated locations (Table 2). As depicted in Fig. 9, these swell events cover a wide range of frequencies and actually arrived at the observation site over 4 days. This is due to the travel distance of each example swell. Values of d were 380, 918, and 4995 km for groups 8, 21, and 44, respectively. Predicted source locations for these three groups appear on the 25 February 1992 (0600 UTC) weather chart reconstruction in Fig. 12. The predicted regions correspond to the locations of three distinct atmospheric low-pressure storms scattered throughout the North Pacific Ocean. The identified source positions are precisely located where the cyclonically rotating winds would be expected to generate waves: in areas of sufficient fetch with winds directed toward the wave observation site.

Specific group 44 is especially interesting, with swell that traveled almost 5000 km over 4 days before reaching the observation site with a strong dispersive signal. The $\overline{f}$, $\overline{\theta}$, and h_s records from group 44 appear in Fig. 13. Unlike some systems, which exhibited varying di-

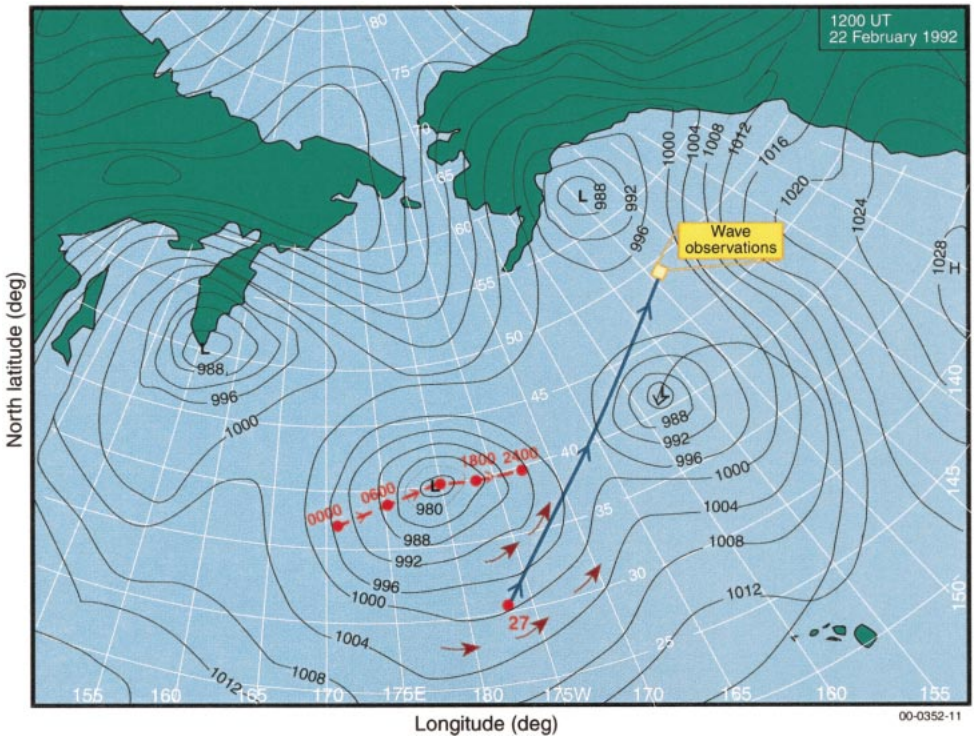

FIG. 11. National Weather Service surface pressure chart for 1200 UT 22 Feb 1992. Predicted source location and great circle propagation routes are displayed for specific group 27.

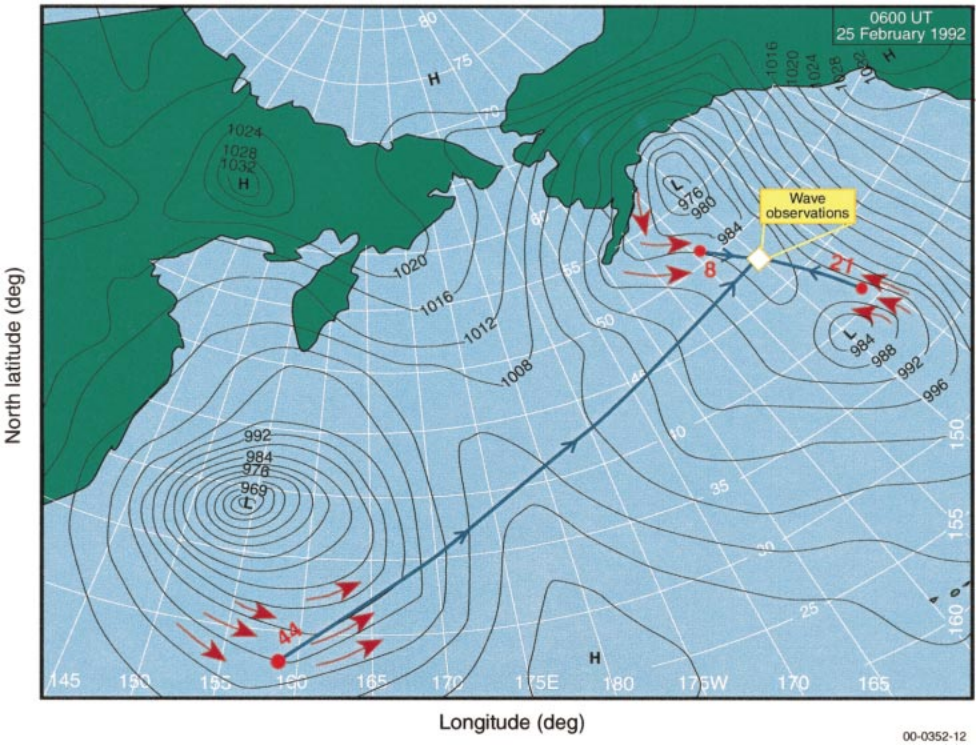

FIG. 12. National Weather Service surface pressure chart for 0600 UTC 25 Feb 1992. Predicted source locations and great circle propagation routes are displayed for specific groups 8, 21, and 44.

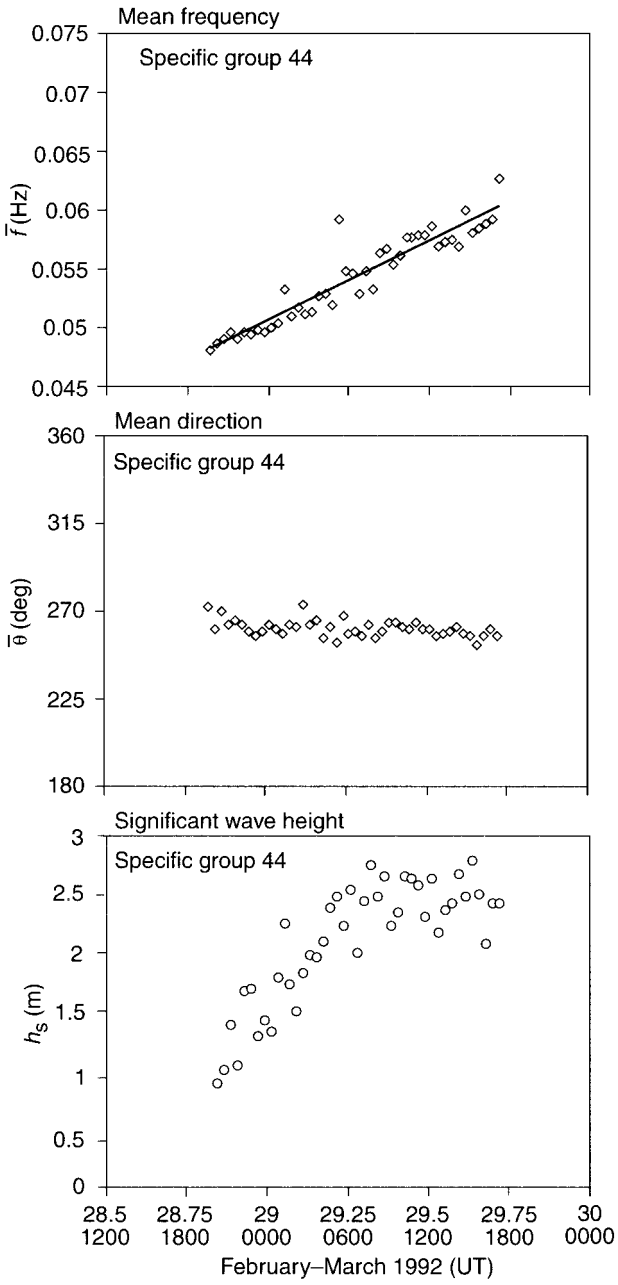

FIG. 13. Evolution of wave frequency, direction, and height statistics for specific group 44 swell partitions.

rections, the directions of group 44 observations have little variance. This is attributed to the source storm's comparatively slow translation speed of approximately 45 km h^{-1} to the east. Group 44 h_s exhibited a rapid increase over the first 9 h and then leveled off at approximately 2.5 m until the end of our observation period. It should be noted that the system 44 observations end because our experiment was over and the wave buoy was retrieved. Examination of NOAA buoy data (#46003) at 51°51′N, 155°54′W indicates the swell of system 44 persisted through the following day. System

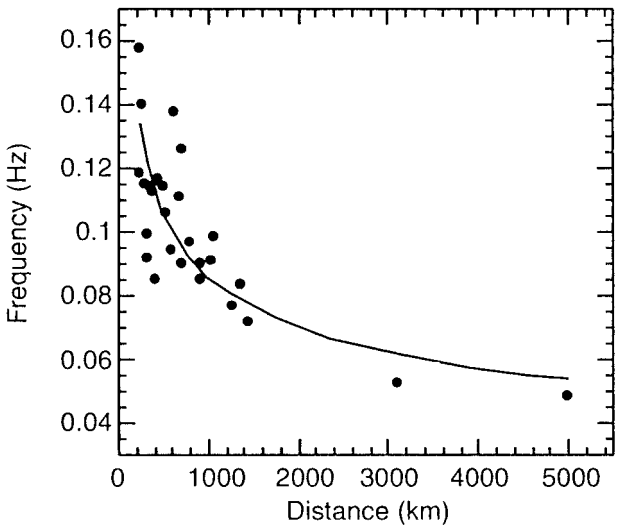

FIG. 14. Frequency downshifting of evolving swells. The lowest observed frequency of each directly detected specific swell system appears as a function of source distance.

44 waves were of such low period that they were not visually detected at the time of the observation. Their existence went unsuspected until post-test processing of the buoy data was completed and the results were validated with the NWS weather charts.

5. Discussion

The wave identification and tracking results provide a synoptic view of wave evolution in the North Pacific Ocean. Casual inspection of Fig. 9 indicates that steeply sloped ''local'' swell events tend to be at higher frequencies and that the more gradually sloped ''older'' events are biased toward lower frequencies. To elucidate this observation, Fig. 14 compares the lowest observed frequency f_1 of each directly detected specific group (Table 2) with source distance d. A distinct trend, given by $f_1 = 0.68\ d^{-0.3}$ ($r = 0.78$), indicates that swell frequency downshifts along the propagation route with the shift rate strongest near the source. The scatter exhibited by the observations is probably due to differences in source strength of the various generation events. The trend exhibited in Fig. 14 is likely an open-ocean demonstration of the energy transfers that result from weak resonant wave–wave interactions (Phillips 1977). Such interactions, included as a nonlinear source term in the wave evolution model WAM (Komen et al. 1994), are strongest for spectral components close in wavenumber. Hence, spectral shifts occur most rapidly near the generation region before dispersion has acted to separate these components in space. As pointed out by a reviewer, higher frequency swells are also more likely to be attenuated through interactions with other wave fields along their propagation paths.

The evolving wave field at the Gulf of Alaska site is

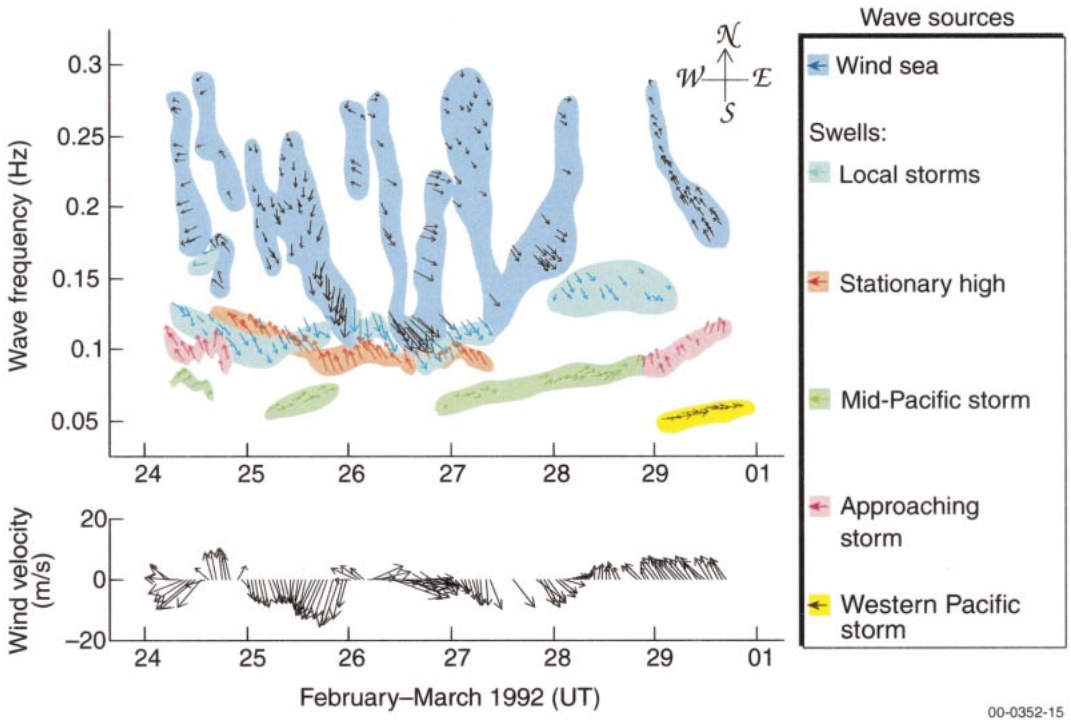

FIG. 15. Wind and wave vector history from Gulf of Alaska observations. To simplify presentation of data, observations were subsampled at a 1-h interval. Gaps in the record apparent on 27 Feb are a result of the WAVEC buoy drifting out of telemetry range. See text for further explanation.

conveniently presented in the form of an hourly wind and wave vector history appearing in Fig. 15. The lower panel portrays the local wind forcing history as recorded by the MINIMET meteorological buoy. Wind vectors indicate the direction toward which the air is moving. The upper panel depicts the evolution of the principal wind sea and swell wave systems over the observation period. Each preliminary wave group exhibits a different shading; the sources of each group (identified in the legend of Fig. 15) were obtained from the weather map verifications of swell source predictions discussed previously. Figure 15 provides a discernible account of the surface roughness history during the observation period. The evolution of up to three simultaneously occurring swell systems in conjunction with the comparatively rapid response of the sea surface to local wind forcing is clearly illustrated.

A few features of Fig. 15 are of particular interest. The build-up and decay of local wind events produces a V-shaped wind sea vector pattern. This pattern is most distinct when winds are steady in direction. Only the ''growth'' side of the V shape appears when winds rapidly change after a development period. This is illustrated by the wind event on 25 February, where a passing front early on 26 February produces an abrupt wind shift of approximately 90°. The result is an immediate transformation of an energetic wind sea into swell. Further analyses of the wind sea observations appear in Hanson and Phillips (1999).

Swell events evolve much more slowly than the rapidly responding wind seas. For a 2.5-day period starting late on 24 February, two series of opposing swells, one from the continual passage of local storms through the Gulf of Alaska and a second from the semistationary atmospheric high pressure system to the southeast, evolve within the same band of frequencies (~0.09–0.13 Hz). The rapid termination of these two events on 27 February results from a gap in the wave record. As discussed previously, the blocking high moved out of the area during this time. After the record gap, the local storm swell is again observed; however, the waves from the stationary high are absent. In contrast to the occurrence of multiple wave systems within a narrow frequency band, on 29 February, three wave systems evolved through the area with widely separated mean frequencies. These consisted of a developing wind sea, swell from an approaching storm to the south, and very low frequency swells from the nearly 5000-km distant western Pacific storm (system 44 in Table 2 and Fig. 9).

6. Conclusions

An approach for wave spectral partitioning, swell tracking, and storm source identification was developed to describe wave evolution in complex wave environments. Until now, identification of swell source times and locations from directional wave spectra was a la-

borious manual procedure (Mettlach et al. 1994). The process is automated here, with a convenient isolation of separate wind sea and swell system statistics from temporally distributed directional wave spectra. The complete set of analysis tools, developed in the Matlab programming environment, are collectively assimilated as the Wave Identification and Tracking System (WITS).

These tools were employed to examine the dynamic wave field in the Gulf of Alaska during winter. The wave conditions at a given site are a combination of wind sea and swell from nearby storms as well as swell from weather events from 500 to 5000 km or more distant. At any given time, the local wind seas are accompanied by up to three or more distinct swell events, with most of the swell energy arriving from southerly to westerly directions. A synthesis of results from the separate swell and wind sea investigations, appearing in Fig. 15, provides a distinct representation of the surface wave history over the duration of the experiment.

There are several potential applications for the wave partitioning and tracking techniques. These tools could provide a convienient interactive display capability for real-time wave observations and models exhibited on the World Wide Web. The methods could be readily extended to the spatial domain for the reduction and display of large datasets such as those from satellite observations and global wave evolution models. In more recent studies, we have extended these methods by ray-tracing the isolated swells in a forward prediction mode. Hence, WITS has a potentially important application in the forecasting of storm waves for shipping routes and populated coastal regions. Furthermore, WITS could be an important tool in the evaluation of wave modeling capabilities. For example, WITS can be used to locate the source of modeling errors, such as a missed storm, poorly specified local winds, or miscalculated swell dissipation. With the recent and planned profusion of global wave observations and simulations, more efficient data reduction and interpretation methods, such as the approaches described herein, will need to be implemented on grand scales.

Acknowledgments. This research was supported by the Office of Naval Research (Ocean Acoustics Code 320A) under Grants N00014-95-1-0078 and N00014-97-1-0075 and by the Space and Naval Warfare Systems command (PMW 182-22). Additional support for the writing of this manuscript came from a JHU/APL Stuart S. Janney Fellowship. We are grateful to Richard Marsden (Royal Military College of Canada) for providing the wave buoy data and to Larry White (JHU/APL) for processing the meteorological data. We appreciate valuable discussions with David Farmer (IOS), Hans Graber (RSMAS), and Susanne Hasselmann (Max-Planck-Institut für Meteorologie). We appreciate an insightful early review of this manuscript by Steve Mack (JHU/APL). Furthermore, we thank the anonymous reviewers for helpful suggestions and, in particular, additional ideas for potential applications of WITS.

APPENDIX

Statistics File Contents

Note: Deep water wave propagation is assumed.

- Observation time (Julian day fraction)
- Partition number
- Total energy, given by (8)
- Root-mean-square wave amplitude

$$a_{\text{rms}} = 1.414\sqrt{e} \tag{A1}$$

- Significant wave height

$$h_s = 4\sqrt{e} \tag{A2}$$

- Mean frequency

$$\overline{f} = \frac{e}{\displaystyle\int_f \int_\theta \frac{S(f, \theta)}{f}\, \partial\theta\, \partial f} \tag{A3}$$

- Mean direction

$$\overline{\theta} = \tan^{-1}\left(\frac{\overline{\sin\theta}}{\overline{\cos\theta}}\right), \tag{A4}$$

where

$$\overline{\sin\theta} = \frac{\displaystyle\int_f \int_\theta S(f, \theta) \sin\theta\, \partial\theta\, \partial f}{e}$$

$$\overline{\cos\theta} = \frac{\displaystyle\int_f \int_\theta S(f, \theta) \cos\theta\, \partial\theta\, \partial f}{e}$$

- Wave age

$$\frac{c_{\text{p}}}{U_{10}} = \frac{g}{2\pi f_{\text{p}} U_{10}} \tag{A5}$$

- Significant slope (Huang 1986)

$$\Psi = \frac{h_{\text{s}}}{\lambda_{\text{p}}} = \frac{2\pi f_{\text{p}}^2 h_{\text{s}}}{g}, \tag{A6}$$

where the peak wavelength

$$\lambda_{\text{p}} = \frac{g}{2\pi f_{\text{p}}^2} \tag{A7}$$

- Directional spread (Yamartino 1984)

$$\sigma = (1 + 0.1547\varepsilon^3) \sin^{-1}\varepsilon, \tag{A8}$$

where

$$\varepsilon = [1 - (\overline{\sin\theta^2} + \overline{\cos\theta^2})]^{1/2}$$

- Angle between wind sea and swell

$$\theta_{s-ws} = |\overline{\theta}_s - \overline{\theta}_{ws}|, \quad \text{(A9)}$$

where the ''s'' and ''ws'' subscripts denote swell and wind sea, respectively. This calculation is performed such that the result is always the minimum angle between the two wave systems.

REFERENCES

Barber, N. F., and F. Ursell, 1948: The generation and propagation of ocean waves and swell. I: Wave periods and velocities. *Philos. Trans. Roy. Soc. London,* **240A,** 527–560.

Bartsch, H.-J., 1974: *Handbook of Mathematical Formulas.* Academic Press, 528 pp.

Earle, M. D., K. A. Bush, and G. D. Hamilton, 1984: High-height long-period waves generated by a severe storm in the northeast Pacific Ocean during February 1983. *J. Phys. Oceanogr.,* **14,** 1286–1299.

Farmer, D. M., 1992: Cruise Report CSS *John P. Tully,* 17 February to 6 March 1992, in Critical Sea Test 7, Phase II Quick-Look Report. The Johns Hopkins University Applied Physics Laboratory, Tech. Rep. STD-R-2119, 216 pp.

Gerling, T. W., 1992: Partitioning sequences and arrays of directional ocean wave spectra into component wave systems. *J. Atmos. Oceanic Technol.,* **9,** 444–458.

Hanson, J. L., 1996: Wind sea growth and swell evolution in the Gulf of Alaska. Ph.D. dissertation, The Johns Hopkins University, 151 pp.

——, and L. H. White, 1991: Assessment of the air–sea boundary zone during Critical Sea Test 4. Johns Hopkins University Applied Physics Laboratory Tech. Rep. STD-R-1978, 116 pp.

——, and F. T. Erskine, 1992: An experiment to study the influence of the air–sea boundary zone on underwater acoustic reverberation. *Proc. MTS '92,* Vol. 2, Washington, DC, Marine Technology Society, 835–847.

——, and O. M. Phillips, 1999: Wind sea growth and dissipation in the open ocean. *J. Phys. Oceanogr.,* **29,** 1633–1648.

——, L. H. White, M. Kennelly, and R. M. Giannola, 1993: Air–sea and upper ocean dynamics during CST-7 Phase 2. Johns Hopkins University Applied Physics Laboratory Tech. Rep. STD-R-2281, 74 pp.

Hasselmann, S., K. Hasselmann, and C. Bruning, 1994: Extraction of wave spectra from SAR image spectra. *Dynamics and Modelling of Ocean Waves,* G. J. Komen et al., Eds., Cambridge University Press, 391–401.

Huang, N. E., 1986: An estimate of the influence of breaking waves on the dynamics of the upper ocean. *Wave Dynamics and Radio Probing of the Ocean Surface,* O. M. Phillips and K. Hasselmann, Eds., Plenum Press, 295–313.

IAHR Working Group on Wave Generation and Analysis, 1989: List of sea-state parameters. *J. Waterw., Port, Coastal, Ocean Eng.,* **115,** 793–808.

Juszko, B.-A., R. F. Marsden, and S. R. Waddell, 1995: Wind stress from wave slopes using Phillips equilibrium theory. *J. Phys. Oceanogr.,* **25,** 185–203.

Kline, S. A., and J. L. Hanson, 1995: Wave identification and tracking system. Johns Hopkins University Applied Physics Laboratory Tech. Rep. STD-R-2436, 44 pp.

Komen, G. J., L. Cavaleri, M. Donelan, K. Hasselmann, S. Hasselmann, and P. A. E. M. Janssen, 1994: *Dynamics and Modeling of Ocean Waves,* Cambridge University Press, 532 pp.

Marsden, R. F., and B.-A. Juszko, 1987: An eigenvector method for the calculation of directional spectra from heave, pitch and roll buoy data. *J. Phys. Oceanogr.,* **17,** 2157–2167.

Mettlach, T., D. Wang, and P. Wittmann, 1994: Analysis and prediction of ocean swell using instrumented buoys. *J. Atmos. Oceanic Technol.,* **11,** 506–524.

Munk, W. H., G. R. Miller, F. E. Snodgrass, and N. F. Barber, 1963: Directional recording of swell from distant storms. *Philos. Trans. Roy. Soc. London,* **255A,** 505–584.

Phillips, O. M., 1977: *Dynamics of the Upper Ocean.* Cambridge, Cambridge University Press, 336 pp.

——, 1985: Spectral and statistical properties of the equilibrium range in wind-generated gravity waves. *J. Fluid Mech.,* **156,** 505–531.

Shumway, R. H., 1988: *Applied Statistical Time Series Analysis.* Prentice-Hall, 379 pp.

Smith, S. D., 1988: Coefficients for sea surface wind stress, heat flux, and wind profiles as a function of wind speed and temperature. *J. Geophys. Res.,* **93,** 15 467–15 472.

Snodgrass, F. E., G. W. Groves, K. F. Hasselmann, G. R. Miller, W. H. Munk, and W. H. Powers, 1966: Propagation of ocean swell across the Pacific. *Philos. Trans. Roy. Soc. London,* **259A,** 431–497.

Tyler, G. D., 1992: The emergence of low-frequency active acoustics as a critical antisubmarine warfare technology. *Johns Hopkins Appl. Phys. Lab. Tech. Dig.,* **13,** 145–159.

Voorrips, A. C., V. K. Makin, and S. Hasselmann, 1997: Assimilation of wave spectra from pitch-and-roll buoys in a North Sea wave model. *J. Geophys. Res.* **102,** 5829–5849.

Yamartino, R. J., 1984: A comparison of several ''single-pass'' estimators of the standard deviation of wind direction. *J. Climate Appl. Meteor.,* **23,** 1362–1366.

Notice to authors: One of the following statements, whichever is appropriate, must be signed by all authors (use multiple forms if needed) of a manuscript and received by the chief editor to which the manuscript is submitted. See "AMS Authors' Guide" on the AMS Web site: http://www.ametsoc.org/AMS/pubs/ag_docs/ag_mainpage.html. Requests for further information should be addressed to American Meteorological Society, 45 Beacon Street, Boston, MA 02108 (e-mail: amspubs@ametsoc.org).

AGREEMENT TO TRANSFER COPYRIGHT
(For non–U.S. government)

Copyright to the article entitled_____

_____

by_____
assigned and transferred exclusively to the American Meteorological Society (hereinafter referred to as AMS) effective if and when the article is accepted for publication
in_____
or in any other AMS journal in which the article may be published with the authors' consent. The authors, however, reserve 1) all proprietary rights other than copyright, such as patent rights, and 2) the right to use all or part of this article in future lectures, press releases, and reviews of their own. Certain additional reproduction rights are granted by sections 107 and 108 of the U.S. Copyright Law. All other uses will be subject to the limitations given in the copyright statement of the AMS journal in which the article is published. To be signed by all authors or if the manuscript is a "work made for hire," by the employer, who is the "legal author" under the U.S. Copyright Law.

Signature	Signature
Print name	Print name
Title if signed by employer	Title if signed by employer
Date	Date
Signature	Signature
Print name	Print name
Title if signed by employer	Title if signed by employer
Date	Date

Note: The form below is to be used for a work of the U.S. government for which copyright protection is not available under Title 17, Section 105. A work of the U.S. government is a work prepared by an officer or employee of the U.S. government as part of this person's official duties.

CERTIFICATION OF U.S. GOVERNMENT MANUSCRIPT

The article entitled_____

_____

by _____
is hereby certified to be a work of the U.S. government, to have been prepared by the author(s) as officer(s) or employee(s) of the U.S. government as part of the author(s) official duties, and therefore to be precluded from copyright protection. It is further certified that the article has not been published previously in any language and it is agreed to promptly notify the chief editor if the manuscript is submitted for publication elsewhere before its disposition by the American Meteorological Society.

Signature	Signature
Print name	Print name
Title if signed by employer/U.S. government agency	Title if signed by employer/U.S. government agency
Date	Date
Signature	Signature
Print name	Print name
Title if signed by employer/U.S. government agency	Title if signed by employer/U.S. government agency
Date	Date